Vibrational density of states of free and embedded semiconducting GaN nanoparticles

P Desmarchelier, K Termentzidis, A Tanguy

Vibrational density of states of free and embedded semiconducting GaN nanoparticles

P Desmarchelier[1,2], K Termentzidis[1], A Tanguy[2]

[1] Universite de Lyon, CETHIL, INSA-Lyon, CNRS UMR5008, F-69621, Villeurbanne, France

[2] Universite de Lyon, LaMCoS, INSA-Lyon, CNRS UMR5259, F-69621, Villeurbanne, France

E-mail: konstantinos.termentzidis@insa-lyon.fr

Abstract. The impact of the size of free and embedded GaN nanoparticles on vibrational properties has been studied using 3 different numerical methods. The thermal conductivity of free nanoparticles was also estimated with Equilibrium Molecular Dynamics. Important discrepancies between the vibrational density of states of small nanoparticles compared to the bulk are observed, such as the presence of modes in the bandgap related to the surface modes, the optical peaks decrease, and the redshift of transverse acoustic peak. When these nanoparticles are embedded in a SiO_2 matrix, the peaks in the bandgap disappear and the transverse acoustic modes are shifted back to the bulk frequencies. These differences between the free and the embedded nanoparticles tend to disappear for nanoparticles with diameters larger than 5 nm. Finally, the thermal conductivity for free nanoparticles is computed, showing a nonlinear augmentation upon the increase of the size of nanoparticles. The latter results could be useful in effective medium models used to estimate the thermal conductivity of nanocomposites.

Submitted to: *Semicond. Sci. Technol.*

1. Introduction

Nanoparticles (NPs) consist of a group of nanomaterials with characteristic dimensions of few nanometers and usually a narrow range of size distribution. Thanks to the evolution of nanofabrication methods it is possible to control their sizes, chemical composition and orientation as well as their dispersion characteristics. They can be integrated into a liquid solution [1] or embedded in a solid matrix [2]. There are several studies in the last two decades which show an increasing interest in the topic, notably the influence of embedding NPs in a matrix. For instance, in nanofluids, the viscosity, the electrical conductivity and the density have been found to change with NPs concentration [3]. Metallic NPs have been used to increase the electrical conductivity of polymers [4]. NPs have been proposed also for specific applications, for example nanoplasmonics where metallic NPs are used for coupling electromagnetic and mechanical waves [5, 6].

The impact of NPs on the thermal transport starts to attract the scientific interest; from the computation of the thermal properties of the NPs themselves, to their impact on the thermal properties in nanocomposites. Studies showed that the thermal conductivity of single silicon NP represents only a fraction of the bulk conductivity and increases linearly with the diameter [7, 8]. When the NPs are embedded in a matrix, the effective thermal properties are altered considerably. The role of NPs as scatterers for the heat carriers has been observed [9], but their influence is not trivial: their orientation [10], stiffness [11], or size distribution [12] can have a strong impact on the thermal properties of these nanocomposites.

Concerning the vibrational properties of NPs, they have been first computed using the continuum mechanics solution for the vibrations of a free sphere [13]. This approach was successfully applied to predict resonant modes in NPs down to 1 nm in diameter for crystalline NPs [14]. This approximation should theoretically work for amorphous NPs as long as characteristic lengthscales of the vibrational modes are not smaller than 40 interatomic distances [15]. Transpositions of the original solution exist for anisotropic materials [16] or embedded NPs [17, 18]. These models based on Lamb's model [19], predict resonant frequencies depending on the material, that scale with the diameter. NPs vibrational properties have been also studied using atomistic models, like molecular dynamics (MD) simulations, with a successful comparison with the continuum theory in the case of Ge or Ag [17, 18]. Some studies have focused on other features of NPs vibrational density of states (VDOS), like spectral spreading and surface effects. These effects were observed in the case of monoatomic metal and bimetallic alloys [20, 21]. The case of III-V semiconductors has been studied by Han and Bester [22, 23], showing similar size effects on NPs VDOS. Finally, II-VI semiconductors NPs have been also studied with a focus on the temperature, size and composition impact on the heat capacity and structural properties [24, 25].

Here MD simulations is used to study the impact of the size of GaN NPs, and whether they are free or embedded in an amorphous SiO_2 matrix, on their VDOS. In

the following section, the description of the modeling of our configurations and the methodologies to compute the VDOS and the thermal conductivity will be detailed. Section 3 gathers the results of VDOS and participation ratio of free and embedded NPs as well as the thermal conductivity of free NPs. The article ends with the Discussion and Conclusion section in which a comparison of the three VDOS methodologies is analysed.

2. Materials and methods

2.1. Modeling of the configurations

To create the GaN NPs, we cut them out from a relaxed GaN wurztite crystal. Hereafter, GaN NPs will be referred simply as NPs. Studied NPs radii R ranges between 1 and 4 nm, and contain 369 to 23 000 atoms, and they will be labeled as NP_R. The free NPs (FNPs) are relaxed in an equilibrium position using a conjugated gradient method, then equilibrated at 300 K for 20 ps. We use fixed boundary conditions for the simulation box to avoid any artefact due to periodic boundary conditions, such as interactions between neighboring NPs. To model the embedded NPs (ENPs) in a silica matrix a cubic simulation box with length twice this of the NP diameter was cut out in a bulk a-SiO_2 sample. The box length was chosen here to limit the interactions between neighboring NPs through periodic boundary conditions while limiting the total number of atoms. In this cubic box a spherical pore with a radius larger than the radius of the NPs by 0.1 Å is cut to avoids any superposition of atoms of the matrix with atoms of the NP. Inside this empty pore, we then added the NP, which has been carved out from the bulk GaN crystal. To relax the interfacial stresses, an additional relaxation is performed using the conjugated gradient method. After this step, the system is annealed at 300 K for 20 ps. All modeling and MD simulations are performed using the opensource software LAMMPS [26]. Two configurations representing the two types of materials studied are depicted in figure 1. The Tersoff interaction potential developed by Kioseoglou *et al.* [27] is used to describe the interatomic interactions. It combines interatomic potential developed: for SiO_2 [28], for GaN [29], for oxynitrides [30] and for silicon nitride [31]. This combined interatomic potential allows the simulations of silica and gallium nitride nanocomposites using the same potential form and it has been used previously with success [10].

The silica glass sample is obtained through the method described by Mantisi *et al.* [33]. A sample of cristobalite crystal is first created and then relaxed to minimize the potential energy. It is then heated from 0 K to 5200 K in 1 ns in order to melt it, and then is kept during 10 ps for homogenization at this high temperature. It is finally quenched from 5200 K to 300 K in 1 ns. All these steps are performed using a BKS interatomic potential [34] instead of the Tersoff potential. The use of a Tersoff potential at high temperature leads to silica micro structure with 40% coordination defects (five fold or six fold coordinated Si atoms), whereas at the normal pressure range, almost none of them are expected [35]. We then reverted to the Tersoff potential for the quench from

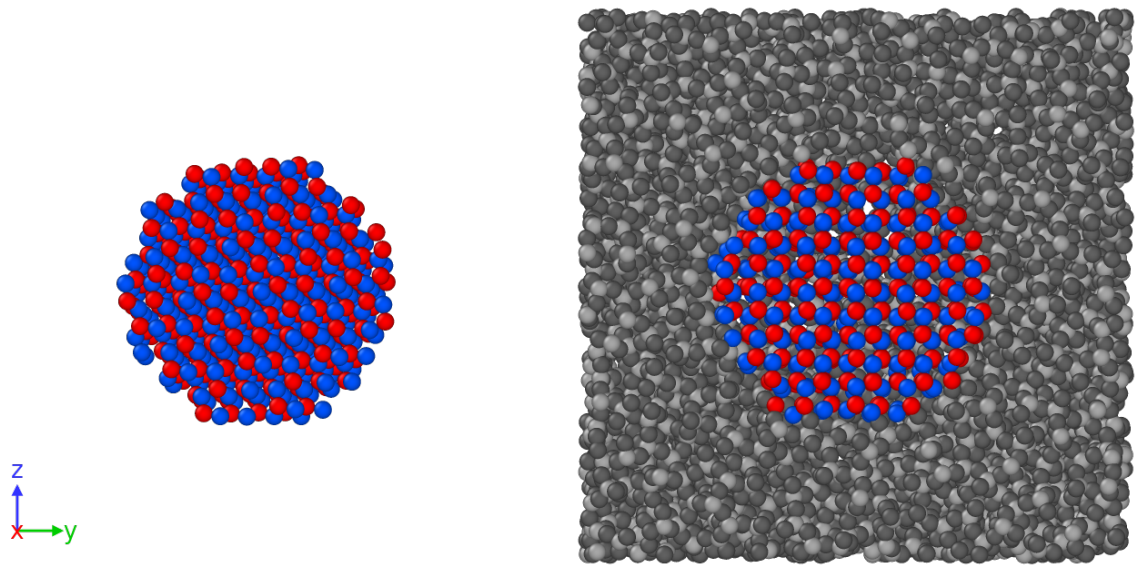

(a) (b)

Figure 1: Visualisation of the free (a) and embedded NPs in silica matrix (b). Blue atoms are Ga, red N, gray Si and dark gray O, obtained with OVITO [32]

300 K to 10 K. Finally we relaxed the structure using a conjugated gradient method and then a Hessian-free truncated Newton algorithm to ensure a better convergence. This method allows to keep the coordination defect below 2%. The partial radial distribution function (PRDF) of the free NPs was examined. The peaks positions and sharpness do not change relative to the bulk PRDF, even for the smallest diameter NP studied here, which is an indication of very small surface reconstruction and amorphization of the free surface of NPs (see Appendix A for more details).

2.2. Vibrational density of states

For the vibrational density of states (VDOS) of free or embedded NPs of different sizes, three methodologies are used here: 1. the direct diagonalization of the dynamical matrix, 2. the eigenvalues estimation with the kernel polynomial method and 3. the Fourier transform of the velocity autocorrelation function.

The first two methods are based on the dynamical matrix (DM). The elements of this matrix are defined for any periodical or finite object as:

$$M_{i\alpha,j\beta} = (\sqrt{m_j m_i})^{-1} \frac{\partial^2 U}{\partial r_{i\alpha} \partial r_{j\beta}} \tag{1}$$

with i and j indexing atoms, α and β indexing the spatial directions, m the masses of the atoms, $r_{j\beta}$ the position of the jth atom displaced in the direction β, and U the potential energy of the system. LAMMPS evaluates the DM by computing the force modification due to a single atomic displacement. The interactions between the atoms are reduced to their stiffness, as the energy landscape is harmonic. The DM associated with the

full system (for FNPs) or only part of it (for ENPs) can be computed. This last one is computed by the motion of every atom belonging to a chosen set. The SiO_2 atoms are fixed, which is equivalent to having a fixed interface around the embedded NPs, allowing the computation of VDOS only for the NPs. The DM describes the vibrations of the NPs with a single $3N \times 3N$ matrix with N the number of atoms. The eigenvalues of this matrix give the eigenfrequencies square of the system and the eigenvectors allows us to obtain the vibrational modes. The handling of the matrix is facilitated by its sparseness: equation 1 reduces to 0 if the atom i lies outside the cutoff radius of atom j.

For the smaller diameters NPs, one can diagonalize explicitly the dynamical matrix using the Implicitly Restarted Arnoldi Method [36] implemented in Sci Py for python. This method will be called "direct" diagonalization of the DM in the following. This method allows obtaining the vibrational modes and the frequencies simultaneously and thus one can compute the participation ratio (PR) for each mode. The participation ratio indicates the fraction of atoms participating to a specific mode. It is computed as:

$$PR = \frac{(\sum_{i=1}^{N} \|r_i\|^2)^2}{\sum_{i=1}^{N} \|r_i\|^4} \frac{1}{N} \tag{2}$$

with r_i the displacement of the ith atom for the specific mode and N the total number of atoms.

Another possibility to compute the VDOS is to use the Kernel Polynomial Method (KPM) described by Weie *et al.* [37] and adapted to the computation of VDOS by Beltukov *et al.* [38]. This method approximates the VDOS by series of Chebyshev polynomials.

The last among the three methods to obtain the VDOS is a statistical method involving the velocity autocorrelation function (VACF) [39]. The system is first thermalized at 50 K for 10 ps with a Nos-Hoover thermostat. The temporal autocorrelation function of the velocities is then averaged over the particles and over the initial time step, using the same thermostat during the next 100 ps. For these simulations, fixed boundary conditions are used for FNPs (that does not include any matrix around) and periodic boundary conditions are used for ENPs (at the borders of the surrounding matrix). The VDOS is then obtained from the temporal Fourier transform of the VACF. Finally, the Fourier transform is filtered with a Savitzky-Golay filter [40]. As the calculation of the VACF relies on statistics, it performs better for large systems over long-time simulation runs. On the other hand, the DM methods allow representing exactly every existing vibrational mode of the simplified (harmonic) system, but are limited to smaller systems due to restrictions related to the numerical diagonalization methods. The KPM method is a good alternative for large systems, but its precision depends on the number of iterations used. The VACF is thus simpler to handle, but less precise for small systems. Moreover, in case of ENPs, the VACF takes into account the atomic motions of the surrounding matrix, while this one is immobile in the DM methods.

2.3. Thermal conductivity

The thermal condutivity of the FNPs is computed thanks to the Equilibrium Molecular Dynamics method. This method is based on the fluctuation dissipation theorem, linking the decay of the fluctuation of an internal variable to its response function. The Green Kubo formula linking the flux auto-correlation integral to the thermal conductivity is written as:

$$\kappa_{\alpha\beta} = (Vk_BT^2)^{-1} \int_0^\infty \langle J_\alpha(0) J_\beta(t) \rangle dt \tag{3}$$

with α and β the directions, V the volume of the NP, k_b the Boltzman constant and $J_\beta(t)$ the heat flux in the direction β at a time t. The heat flux computation entails for each atom a kinetic part and a potential part. The potential part is derived from the virial stress. A discretized version is [41]:

$$\kappa_{\alpha\beta} = \Delta t(Vk_BT^2)^{-1} \sum_{m=1}^{M} (m-p)^{-1} \sum_{n=1}^{p} J_\alpha(m+n) J_\beta(m) \tag{4}$$

with Δt the time step between two successive flux computations, M the total number of time steps, and p the maximum step over which the autocorrelation function is averaged. The inclusions are heated at 300 K, using an initial velocity distribution without overall translational or rotational momentum. The system is then equilibrated at this temperature for 0.5 ns using a Nos-Hoover thermostat. We then extract the flux every 10 fs, and compute the flux autocorrelation decay over 40 ps, while the average is done over 5 to 10 ns. To obtain better statistics, the results are averaged over 5 to 10 runs with different seeds for initial velocities. All these simulations were done at 300 K using a Nos-Hoover thermostat. The NPs were free to move, nevertheless, very few translation or rotation collective movements have been observed. These latter are excluded in the statistics for the computation of κ

There are known issues for the computation of virial stress with many-body potential such as Tersoff potential with LAMMPS, but as discussed by Termentzidis *et al.* [10] we will considered it as marginal.

3. Results

3.1. VDOS of free nanoparticles

The vibrational density of states of FNPs with different sizes (colored plain lines) and for bulk GaN (dashed black line) are depicted in figure 2 for comparison. At first view, one can notice that bulk and NPs VDOS are quite similar, even for small NPs composed of a few hundreds atoms (see table 1). The two acoustic peaks are noticeable and they can be linked to the Van Hove singularities [42]. Then, we will focus on the effect of the diameter reduction. Three main effects appear: the first one is the population of the bandgap, by 3 main modes at 14, 18 and 20 THz. Their intensities increase as the NPs decrease in size. Their relative importance in the DOS spectra is confirmed by the difference in participation ration (PR) for different sizes: between FNP_{10} and FNP_{25}

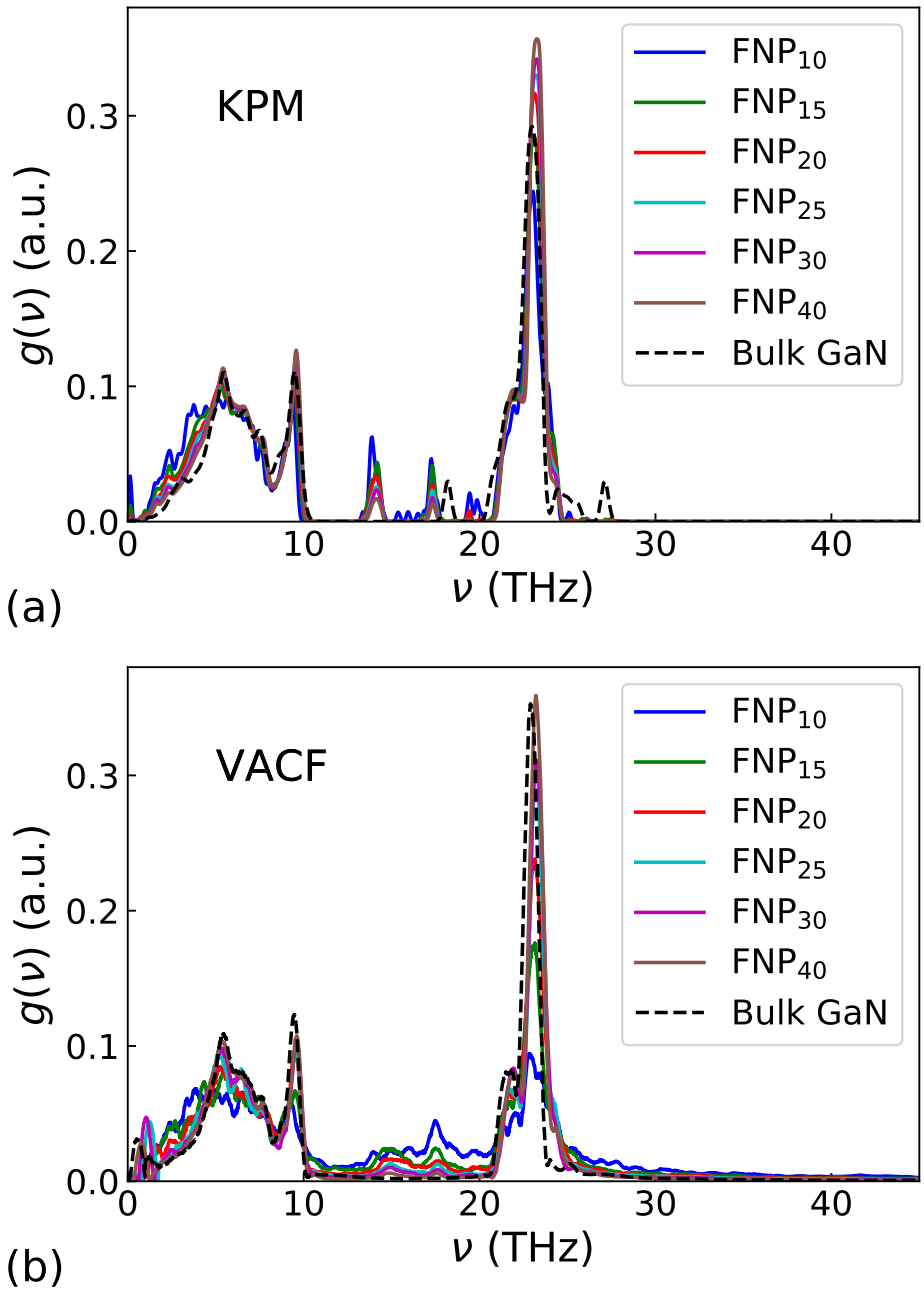

Figure 2: VDOS of GaN FNPs computed from the DM with KPM (a) and from the VACF (b). Colored lines represent the different NPs and the dashed black line the bulk GaN

their PR decreases (see left column of figures 3), indicating that these modes are more and more spatially confined in percentage of in-phase moving atoms. These modes are related to surface modes and they were observed for other III-V semiconductors [22]. The increase of PR of those modes with the increase of the surface to volume ratio (see table 1) tends to confirm their localisation at the surface. It is also worth noticing here that the frequencies of these modes do not depend on the size of NPs. This means that

they cannot be linked to Lamb's modes or other resonant modes. Note also here, that with the VACF method (figure 2 b) the peak at 14 THz is less sharp.

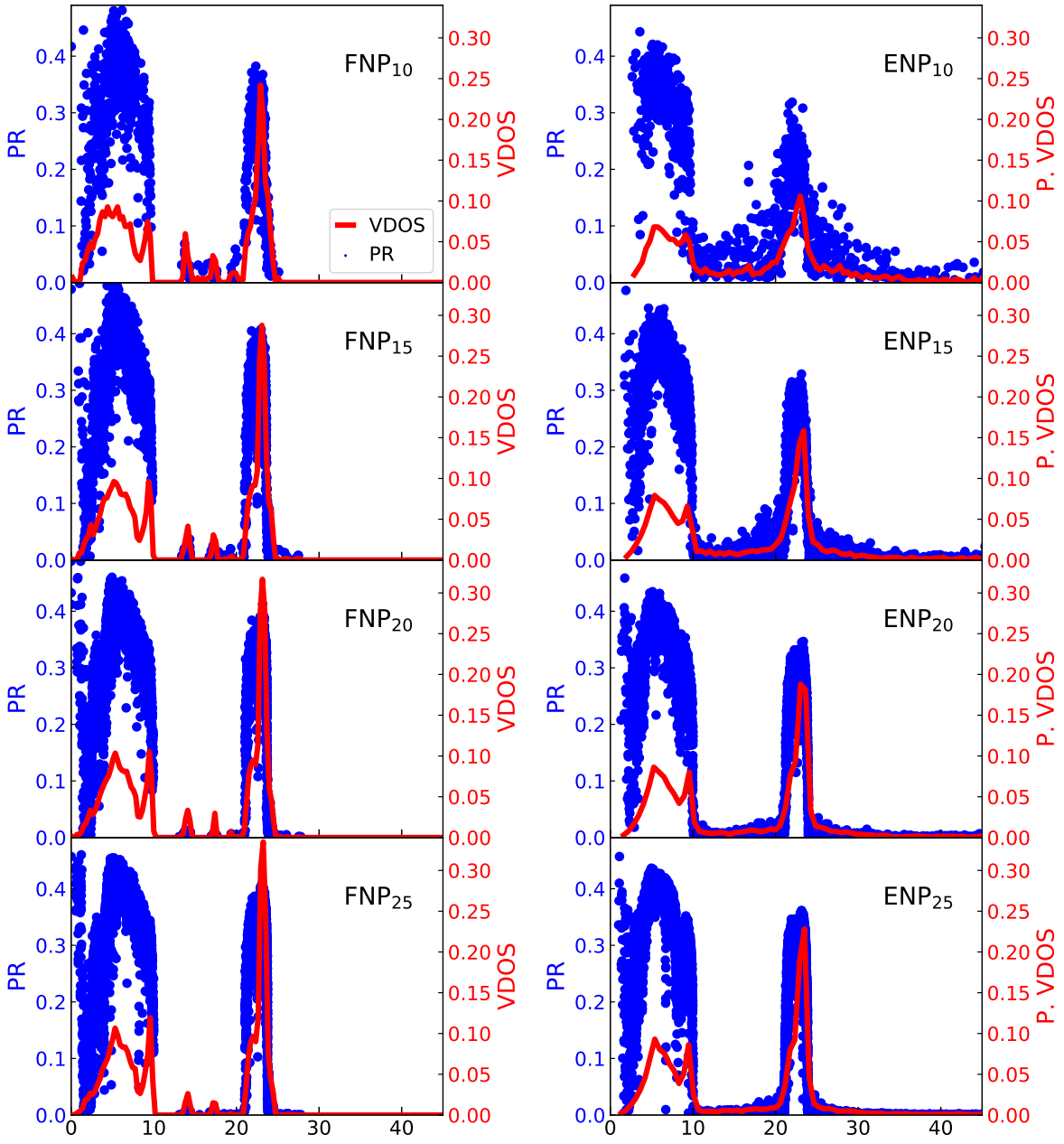

Figure 3: VDOS (red line) and participation ratio (blue dot) derived from the direct diagonalization of the DM for the FNPs (right) and ENPs (left)

The second effect is a redshift and/or blurring of the first acoustic peak for the radii up to 20 Å. This shift increases with decreasing NPs radius. This phenomenon is more sensitive to the VDOS estimation through KPM (figure 2a) and with the direct method (figure 3 left panel), but it is also visible when using the VACF, especially for the smallest NPs (figure 2b). This redshift differs from what was previously observed by Combe *et al.* [17] for Ge nanodots using Stillinger Weber potential. In the latter

work a blue shift was mentioned instead, as it would be expected from the Lamb's theory where the eigenfrequencies scale with the inverse of the radius. Nevertheless, there are other studies that confirm our results; a mode softening. This softening was linked to the increased surface-to-volume ratio for metallic NP [21] or GaP NP [22]. Now concerning the blurring effect, we believe that this is due to the modification of the shape of resonant modes. If we use the longitudinal and transverse sound velocities given by Polian *et al.* [43], the fundamental Lamb's modes of a free isotropic sphere, corresponding to the NPs sizes of our study, lies between 1 and 5 THz. Below 3 THz the wavelength of the longitudinal phonons as described by Jiang *et al.* [44] exceeds largely the smallest NP diameter. But, due to elastic heterogeneities, the effective sound velocity decreases, competing with the decrease in the NPs radius, and thus impacting the Lamb's frequencies [45].

The last diameter-dependent feature of VDOS is the intensity decrease of the optical peaks. A broadening of optical peaks was already observed and attributed to changes in the crystalline structure [22]. But the crystallinity of our NPs does not seem to change (see Appendix A). Moreover, the decrease of optical peaks intensities compared to acoustic ones appears also in the direct diagonalization. Thus, this phenomenon is independent of the method used to calculate the VDOS. The surface effect is the most probable explanation of the intensity decrease, as the ratio of Ga to N is constant for all the NPs.

Last but not least, it is worth to mention at this point, that the optic peaks obtained with this interatomic potential is blue shifted when compared to the one obtained from experimental results [46] and even more compared to *ab-initio* computation [47, 44]. The empirical potential used here shows a good agreement for the acoustic modes but is less accurate for the optic modes. A figure comparing the results from our study, the exprimental [46] and the *ab-initio* [47] results is available in Appendix B.

3.2. Thermal conductivity of FNP

The thermal conductivity (κ) of the FNPs of radii 10, 15, 20, 25, 30 and 40 Å are depicted in figure 4 and recorded in the table 1. We have reported in the same table the percentage of surface atoms, belonging to a spherical shell of 2 Å thickness. 2 Å is chosen in order to encompass every atom appearing visually at the surface.

The κ of NP, as expected, is only a small fraction of bulk GaN one ($\approx$ 160-220 $\mathrm{W\,K^{-1}\,m^{-1}}$ [48]). For the smallest NP studied here, it is three orders of magnitude less than the bulk value. When increasing the size of NP, the κ increases in a non linear way, in contrast to a previous study for Silicon FNPs with diameters 2 to 12 nm in which a linear size dependence was reported [8].

The previously reported VDOS modifications due to the size effect can impact the κ when taking into account the separate contribution of each phonon frequency. For instance, modes below 5 THz contribute to 50% of the thermal conductivity according to Tang *et al.* [47]. Furthermore, the surface modes in the bandgap gain intensity upon

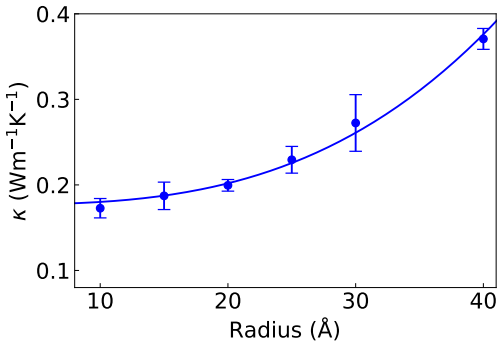

Figure 4: Thermal conductivity of FNPs computed with EMD at 300K, the error bar corresponds to the standard deviation between the 5 to 10 independent runs. The blue line is a fit to a cubic scaling law as a guide to the eye.

	# of atoms	% of surface atom	κ ($\mathrm{W\,K^{-1}\,m^{-1}}$)
NP_{10}	369	52	0.17 $\pm$.01
NP_{15}	1239	36	0.19$\pm$.02
NP_{20}	2952	29	0.20$\pm$.01
NP_{25}	5657	24	0.23$\pm$.02
NP_{30}	9942	20	0.27$\pm$.03
NP_{40}	23580	16	0.37$\pm$.02

Table 1: Characteristics of the FNP

decreasing the radius of NPs. However, these surface modes do not penetrate in the NPs, so they do not contribute much to the overall flux. Size effects are also known to promote phonon mode hybridization that can impact the thermal conductivity [49]. We are aware that the few points in figure 4 cannot give the exact tendency nor the whole picture, but we can notice a cubic scaling dependence of κ with the diameter, which might be related to a volume (r^3) dependence. The calculated thermal conductivity of a FNP here quantifies how effective the energy exchange inside the particle is. Due to size effects, it differs from the bulk. This is an important effect that one should take into account when effective medium approximation (EMA) models are used to estimate the effective κ of a nanocomposite.

3.3. Vibrational density of state of ENP

In the following section the ENP will be studied, focusing on the substitution of the free surface by an interface with an amorphous material. For the case of ENPs, the frequency shift of the VDOS acoustic peaks with the size of the ENPs as observed in the previous paragraph for the FNPs disappears, as well as the modes inside the bandgap of bulk GaN at 14, 18 and 20 THz. We relate these modifications to the elimination of the surface modes [21, 22].

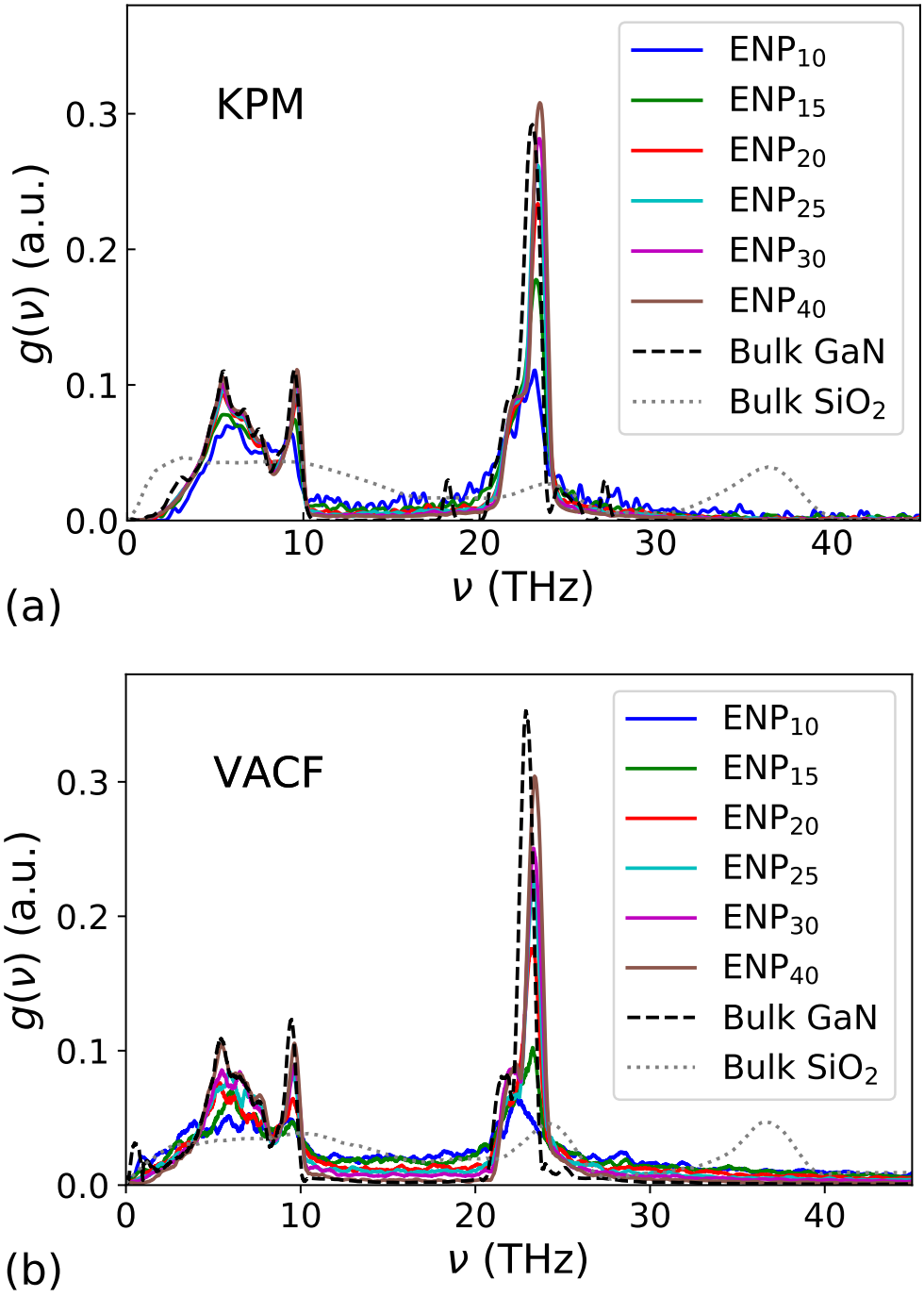

Figure 5: VDOS of GaN ENPs computed with the DM with KPM (a) and from the VACF (b). Colored lines represent the different NPs, the dashed black line the GaN bulk and the dotted gray line the SiO_2.

A marked broadening of the optical peaks can still be observed for the smallest ENPs, as well as a population of the bandgap, but this time in a much more uniform way. This can be understood as the influence of the SiO_2 matrix on the modes. Matrix modes are indeed available at those frequencies as can be seen in figure 5 where the SiO_2

VDOS is represented with a dotted line. Previous work showed that, at the interfaces, modes of the different phases combine together [50, 51, 52]. This effect could be used to deduce which mode can be transmitted or reflected on the inclusion. Additionally, new optical branches seem to appear towards high frequencies for all ENP sizes, something that was not observed for FNP. The most probable explanation for this might be the hybridization of the optical modes of the GaN with the higher frequencies modes of the SiO_2 matrix.

Finally, the only common tendency between free and embedded NPs is the relative decrease of the optical peaks for small sizes. This effect is even more visible in figure 5 compared to figure 2. It is partially due to the normalization of the VDOS area, but the acoustic peaks seem less impacted. As this effect is present for both free and embedded NPs, it cannot be due to free surface effect only. It is most probably related to the amorphization of the surface or interface. Indeed, the embedded NPs seem to show more amorphization than the FNPs, as discussed in Appendix A.

The previous observation on the VDOS of ENPs are valid for the two methodologies VACF and KPM. The last one shows a sharper definition of modes and it is thus selected to make a more rigorous comparison between the ENPs and FNPs VDOS. The comparison between FNPs and ENPs in figure 6 allows underlining the previously cited differences (here represented in red). First the difference in intensity of the optical peaks between the FNPs and ENPs can be observed; the peaks for the ENPs are lower compared to FNPs. This difference is enhanced when decreasing the size of the NPs (red arrows). Then the redshift of the TA peak for FNPs appears clearly for radii up to 20 Å, while the distinct modes in the bandgap for FNPs disappear for the ENPs. This confirms the fact, mentioned in the previous paragraph, that these modes are related to free surface effects. Finally, one can observe in ENPs background modes, which are related to the matrix.

4. Discussion and Conclusion

Let's start this section with an overall comparison of the 3 methods used to simulate the VDOS for both embedded and free NPs. To do so, the VDOS of NPs with two different sizes are depicted in figure 7 for the 3 methods. The estimations of the DOS with the direct diagonalization or the approximation with KPM leed to sharper features in the DOS, especially for the smallest diameters NPs (top panels of figure 7). This can have two origins: the poor statistics of the VACF due to the reduced number of particles, and/or the anharmonicity mainly due to the agitation of surface atoms during simulations. In case of ENPs, the vibrations of the surrounding matrix allowed only in the VACF method, contribute also to broaden the VDOS in this case. For bigger diameters, the similarities between the methods using the DM and the VACF validate the fixed interface conditions used when computing the DM. Finally, this shows that the computation of the DM restricted to the NP atoms only is globally adapted to the computation of VDOS of NPs embedded in an amorphous matrix.

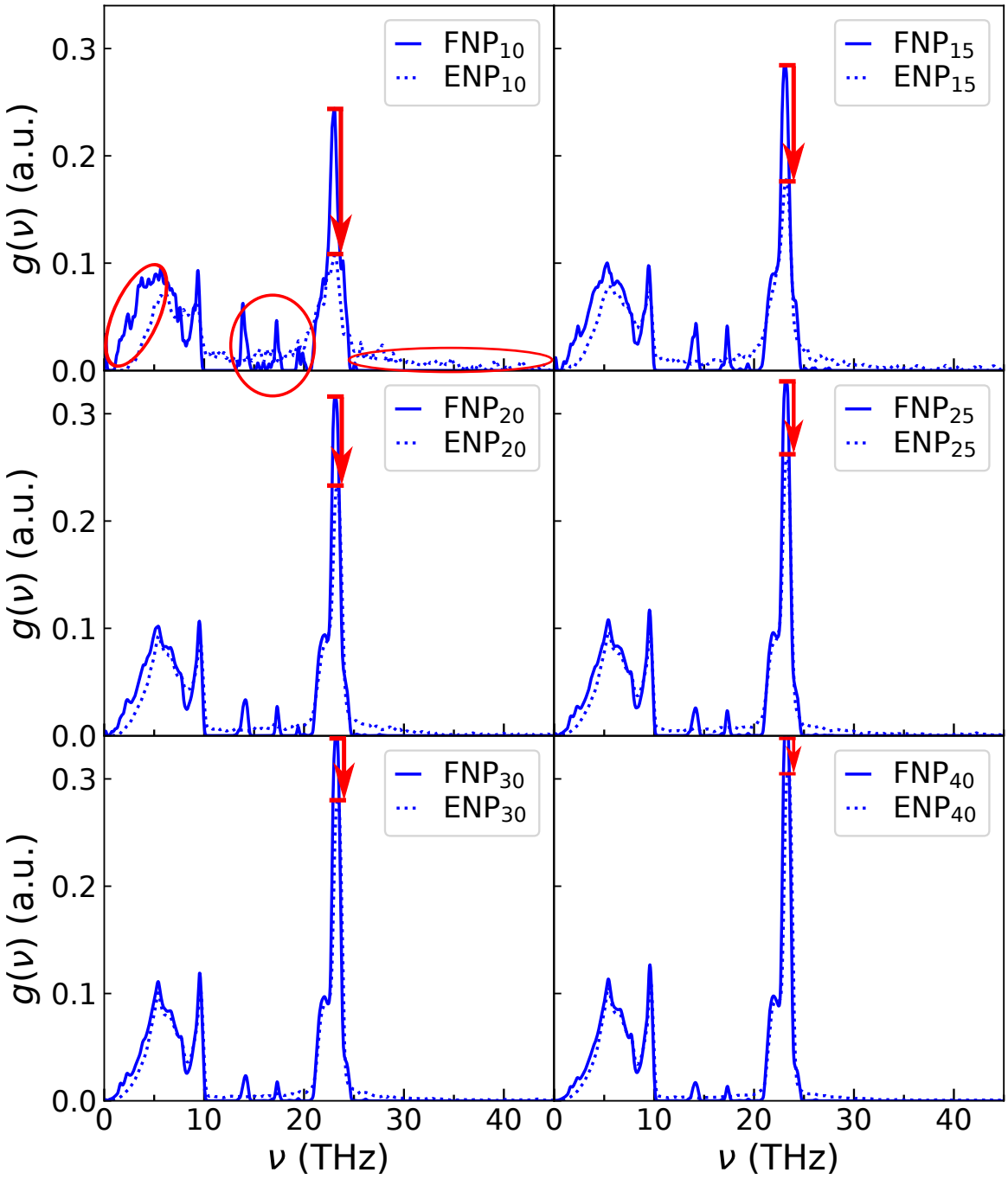

Figure 6: VDOS comparison for every NP diameter between free in continuous line and embedded in dotted line, from the DM using KPM

In general the three methods converge for NPs with diameters larger than 5 nm. Nevertheless, for smaller NPs one should be careful about the methodology selection, as the impact of temperature can only be taken into account directly with the VACF method. On the other hand the DM approach detects detailed features that the VACF looses due to thermal agitation and poor statistics (small number of atoms). We have

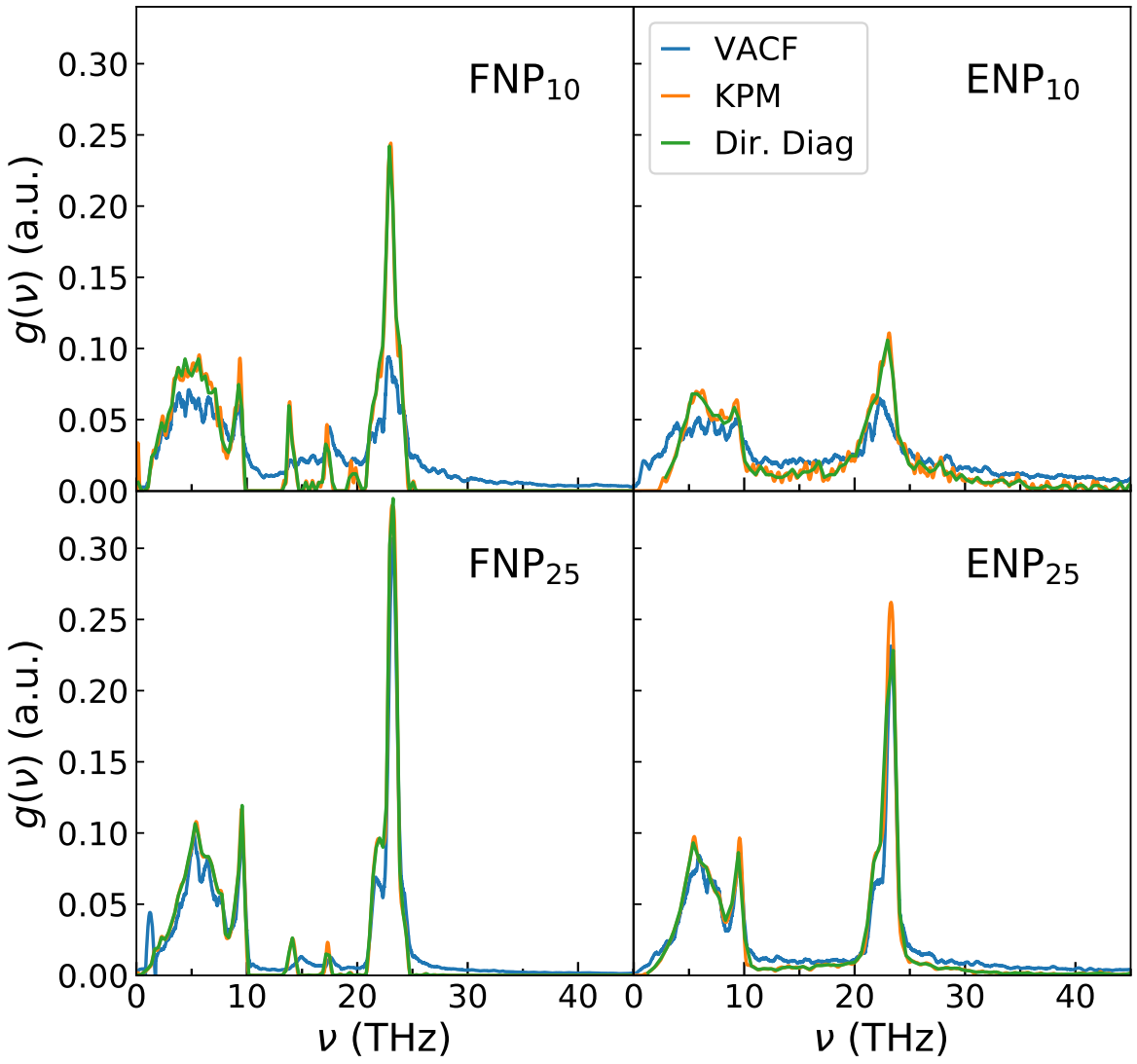

Figure 7: VDOS for NP_{10} and NP_{25} free and embedded, using the different method for the evaluation of the VDOS

to notice here that the DM is feasible only for small NPs with maximum 10 000 atoms because larger number cannot be considered due to CPU limitations related to the direct diagonalization scheme. In contrast KPM, scheme can overpass the direct method limitations, but it is also constrained due to matrix size limitation compared to available RAM.

To conclude, the vibrational density of states of GaN NPs free or embedded in an SiO_2 matrix was studied. We have observed 3 different phenomena for the FNP: a redshift of the first acoustic peak, the appearance of surface modes in the bandgap and an intensity decrease of the optical modes. As the NP is embedded in a SiO_2 matrix, only the latter effect persists, and modes induced by the interface with the matrix increase in intensity as the NPs decrease in size. We did not observe specific peaks for

the Lambs modes characterized by a frequency inversely proportional to the radius of the inclusions: they are indeed hidden in the VDOS spectra, but can be identified easily at low frequencies with the DM.

Concerning the thermal conductivity of the FNPs, we have observed that it does not follow a previous linear dependence observed for the case of silicon NPs. In III-V semiconducting NPs and more specifically in GaN NPs the thermal conductivity increases in a cubic power low of nanoparticles diameter. The nonlinear size dependence of the thermal conductivity underlines that the mean free path limitation to the NPs size is not the only parameter to take into account, otherwise we would have had a linear dependence with the size. This nonlinearity might be due to surface modes and how these modes interact with the heat flux fluctuations in the core of the NP. Note that collective modes involving the full matrix coupled to the nanoparticle are not taken into account by the DM methods due to the fixed condition. It was shown in recent articles that the matrix can also play a role [51], especially from its damping properties [11], together with the impedance break between the particle and the matrix [52]. Collective modes may appear when nanoparticles are embedded in a host matrix. However, our purpose here focuses on the properties of isolated nanoparticles. The thermal properties of the specific nanocomposite (GaN nanoinclusions in a silica matrix) have been already studied and discussed elsewhere [10].

Acknowledgments

This work was granted access to the HPC resources of IDRIS under the allocation 2020-A0070911092 made by GENCI. We would like to thank Professor Joseph Kioseoglou of the Aristotle Universtity of Thessaloniki for all fruitful discussions.

Appendix A. Partial radial distribution function

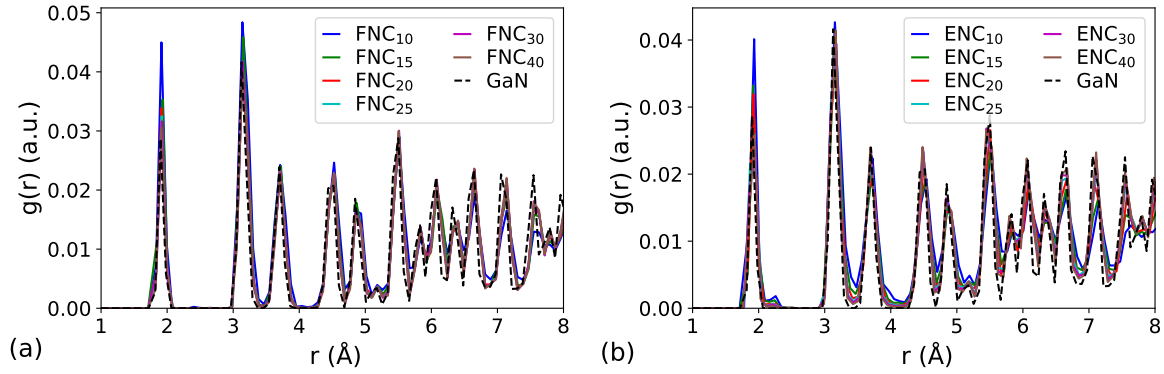

Figure A1: RDF for GaN atoms at 300K for FNP (a) and partial RDF of GaN in ENP (b)

The PRDF of ENPs and FNPs is represented in figure A1. The PRDF allows

comparing the crystalline structure of the NPs with decreasing radius and the differences with the bulk. The first peak represents the distance to the nearest neighbor, the second one the distance to the second nearest neighbor and so one. Here, we see little or no change to the PRDF going from bulk to free NPs. A similar analysis made on Si NPs with a Tersoff potential showed reorganization at the surface [7], this discrepancy may come from the higher temperature (1600K) annealing of their NPs. For the embedded NPs on the opposite, a peak broadening can be observed. It is visible from the second nearest neighbor on. This broadening increases with decreasing diameter which is symptomatic of amorphization at the interface due to the contact with a-SiO_2. These observations confirm that for our configuration, the GaN-SiO_2 interface has more impact on the vibrational properties than the free surface of FNPs.

Appendix B. Comparison of GaN bulk VDOS

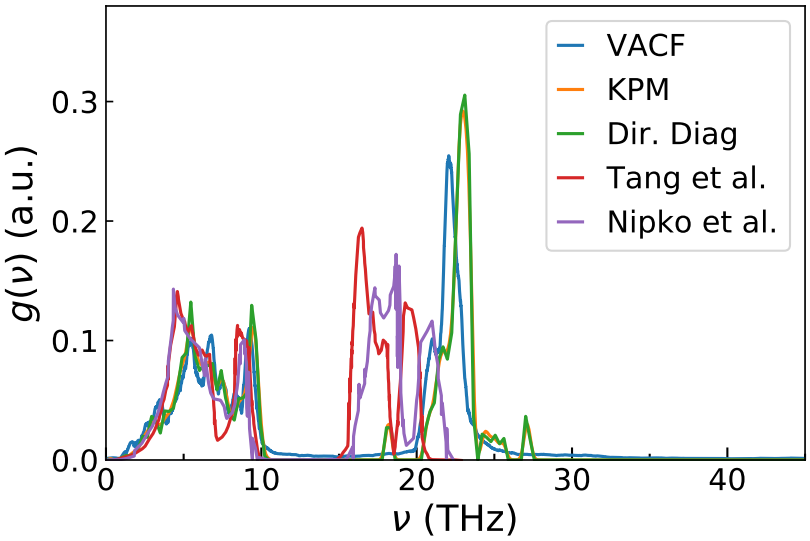

Figure B1: Comparison of the VDOS of bulk GaN using KPM, direct diagonalization and VACF with results from *ab-initio* calculation by Tang *et al.* [47] and experimental results by Nipko *et al.* [46]

References

[1] Qiu L, Zhu N, Feng Y, Michaelides E E, Żyła G, Jing D, Zhang X, Norris P M, Markides C N and Mahian O 2019 *Physics Reports* ISSN 03701573 URL `https://doi.org/10.1016/j.physrep.2019.12.001`

[2] Daudin B 2008 *Journal of Physics Condensed Matter* **20** ISSN 09538984

[3] Nabati Shoghl S, Jamali J and Keshavarz Moraveji M 2016 *Experimental Thermal and Fluid Science* **74** 339–346 ISSN 08941777 URL `http://dx.doi.org/10.1016/j.expthermflusci.2016.01.004`

[4] Del Castillo-Castro T, Larios-Rodriguez E, Molina-Arenas Z, Castillo-Ortega M M and Tanori J 2007 *Composites Part A: Applied Science and Manufacturing* **38** 107–113 ISSN 1359835X

[5] Berweger S, Atkin J M, Xu X G, Olmon R L and Raschke M B 2011 *Nano Letters* **11** 4309–4313 ISSN 15306984

[6] Girard A, Gehan H, Crut A, Mermet A, Saviot L and Margueritat J 2016 *Nano Letters* **16** 3843–3849 ISSN 15306992

[7] Li H P and Zhang R Q 2013 *AIP Advances* **3** ISSN 21583226 URL `https://doi.org/10.1063/1.4818591`

[8] Fang K C, Weng C I and Ju S P 2006 *Nanotechnology* **17** 3909–3914 ISSN 09574484

[9] Nomura M, Shiomi J, Shiga T and Anufriev R 2018 *Japanese Journal of Applied Physics* **57** ISSN 13474065

[10] Termentzidis K, Giordano V M, Katsikini M, Paloura E, Pernot G, Verdier M, Lacroix D, Karakostas I and Kioseogloud J 2018 *Nanoscale* **10** 21732–21741 ISSN 18196608

[11] Tlili A, Giordano V M, Beltukov Y M, Desmarchelier P, Merabia S and Tanguy A 2019 *Nanoscale* **11** 21502–21512 URL `http://dx.doi.org/10.1039/C9NR03952J`

[12] Huang C L, Qian X and Yang R G 2017 *Epl* **117** ISSN 12864854

[13] Eringen A C and Suhubi E 1975 *Elastodynamics* academic ed vol II (New York) ISBN 0122406028

[14] Juvé V, Crut A, Maioli P, Pellarin M, Broyer M, Del Fatti N and Vallée F 2010 *Nano Letters* **10** 1853–1858 ISSN 15306984

[15] Wittmer J P, Tanguy A, Leonforte F and Barrat J L 2002 *Europhysics Letters* **57** 423–429 ISSN 01694332

[16] Saviot L and Murray D B 2009 *Physical Review B - Condensed Matter and Materials Physics* **79** 1–11 ISSN 10980121 (*Preprint* `0904.2959`)

[17] Combe N, Huntzinger J R and Mlayah A 2007 *Physical Review B - Condensed Matter and Materials Physics* **76** 1–12 ISSN 10980121

[18] Murray D B and Saviot L 2004 *Physical Review B - Condensed Matter and Materials Physics* **69** 1–9 ISSN 1550235X

[19] Lamb H 1881 *Proceedings of the London Mathematical Society* **1** 189–212

[20] Sauceda H E, Salazar F, Pérez L A and Garzón I L 2013 *Journal of Physical Chemistry C* **117** 25160–25168 ISSN 19327447

[21] Calvo S R and Balbuena P B 2005 *Surface Science* **581** 213–224 ISSN 00396028

[22] Han P and Bester G 2011 *Physical Review B - Condensed Matter and Materials Physics* **83** 1–8 ISSN 10980121

[23] Han P and Bester G 2012 *Physical Review B - Condensed Matter and Materials Physics* **85** 1–4 ISSN 10980121 (*Preprint* `1202.1634`)

[24] Kurban M, Baris Malcioglu O and Erkoç S 2016 *Chemical Physics* **464** 40–45 ISSN 03010104

[25] Kurban M 2018 *Turkish Journal of Physics* **42** 443–454 ISSN 13036122

[26] Plimpton S 1995 *Journal of Computational Physics* **117** 1–19 ISSN 00219991 (*Preprint* `nag.2347`)

[27] Kioseoglou J, Katsikini M, Termentzidis K, Karakostas I and Paloura E C 2017 *Journal of Applied Physics* **121** ISSN 10897550

[28] Munetoh S, Motooka T, Moriguchi K and Shintani A 2007 *Computational Materials Science* **39** 334–339 ISSN 09270256

[29] Nord J, Albe K, Erhart P and Nordlund K 2003 *Journal of Physics Condensed Matter* **15** 5649–5662 ISSN 09538984

[30] Okeke O U and Lowther J E 2009 Molecular dynamics of binary metal nitrides and ternary oxynitrides URL `http://dx.doi.org/10.1016/j.physb.2009.06.003`

[31] de Brito Mota F, Justo J and Fazzio A 1998 *Physical Review B - Condensed Matter and Materials Physics* **58** 8323–8328 ISSN 1550235X

[32] Stukowski A 2010 *Modelling and Simulation in Materials Science and Engineering* **18** 015012

[33] Mantisi B, Tanguy A, Kermouche G, Barthel E, Mantisi B, Tanguy A, Kermouche G and Barthel E 2012 *Eur. Phys. J. B (2012)* **85** 304

[34] Van Beest B W H, Kramer G J, Shell K and Van Santen R A 1990 1955–1958 URL `https://journals.aps.org/prl/pdf/10.1103/PhysRevLett.64.1955`

[35] Liang Y, Miranda C R and Scandolo S 2007 *Physical Review B* 1–5
[36] Lehoucq R B, Sorensen D C and Yang C 1998 *ARPACK users' guide: solution of large-scale eigenvalue problems with implicitly restarted Arnoldi methods* vol 6 (Siam)
[37] Weiße A, Wellein G, Alvermann A and Fehske H 2006 *Reviews of Modern Physics* **78** 275–306 ISSN 15390756
[38] Beltukov Y M, Fusco C, Parshin D A and Tanguy A 2016 *Physical Review E* **93** 1–18 ISSN 24700053 (*Preprint* 1510.01761)
[39] Dove M 1993 *Introduction to lattice dynamics* vol 136
[40] Savitzky A and Golay M J 1964 *Analytical chemistry* **36** 1627–1639
[41] Schelling P K, Phillpot S R and Keblinski P 2002 *Nanoscale thermal transport Journal of Applied Physics* **80** 2484 URL http://aip.scitation.org/toc/apl/80/14
[42] Van Hove L 1953 *Physical Review* **89** 1189
[43] Polian A, Grimsditch M and Grzegory I 1996 *Journal of Applied Physics* **79** 3343–3344 ISSN 00218979
[44] Jiang Y, Cai S, Tao Y, Wei Z, Bi K and Chen Y 2017 *Computational Materials Science* **138** 419–425 ISSN 09270256 URL http://dx.doi.org/10.1016/j.commatsci.2017.07.012
[45] Tanguy A, Wittmer J P, Leonforte F and Barrat J 2002 *Physical Review B - Condensed Matter and Materials Physics* 1–17
[46] Nipko J C, Loong C K, Balkas C M and Davis R F 1998 *Applied Physics Letters* **73** 34–36 ISSN 00036951
[47] Tang D S, Qin G Z, Hu M and Cao B Y 2020 *Journal of Applied Physics* **127** ISSN 10897550
[48] Jezowski A, Danilchenko B A, Boćkowski M, Grzegory I, Krukowski S, Suski T and Paszkiewicz T 2003 *Solid State Communications* **128** 69–73 ISSN 00381098
[49] Ma, Anufriev, RomanNomura M, Shiomi J and Shiga T 2018 *Japanese Journal of Applied Physics* **57** ISSN 13474065
[50] France-Lanord A, Merabia S, Albaret T, Lacroix D and Termentzidis K 2014 *Journal of Physics Condensed Matter* **26** ISSN 1361648X
[51] Damart T, Giordano V M and Tanguy A 2015 *Physical Review B* **92** 1–11 ISSN 1550235X (*Preprint* 1507.02112)
[52] Luo H, Gravouil A, Giordano V and Tanguy A 2019 *Nanomaterials* **9** ISSN 20794991